JOURNAL OF MATERIALS SCIENCE 21 (1986) 4101–4106

A comparison between ion implantation and laser alloying of iron for oxidation resistance improvement

Part 2 *Aluminium alloying*

M. PONS, M. CAILLET, A. GALERIE
Laboratoire d'Adsorption et Réaction de Gaz sur Solides, UA CNRS 413, ENSEEG-INPG-BP75, 38402 St Martin D'Hères, France

Following previous results concerning boron alloying by ion implantation or laser surface melting, we study the role of aluminium to improve the high temperature oxidation of iron. Laser alloying has a greater efficiency than ion implantation. The aluminium containing phases formed at the metal–scale interface are responsible for the observed protection. The behaviour of the laser surface alloy is quite comparable to that of conventional alloys Fe–5Al. These two techniques, ion implantation and laser irradiation, seem to be of importance for future developments of corrosion protection.

1. Introduction

Surface treatments of metals and alloys allow the modification of the surface of relatively inexpensive substrates by adding small amounts of alloying elements [1–4].

We used ion implantation and laser alloying to increase the thermal oxidation resistance of iron. In a first paper [5], the effects of boron alloying have already been presented; it was shown that both surface treatments have a great efficiency against thermal oxidation of iron.

We present here experimental results concerning the alloying of aluminium into iron using these two techniques and compare the effects on the high temperature oxidation behaviour of iron.

2. Experimental procedure

2.1. Ion implantation

2.1.1. Direct ion implantation

Iron was supplied in form of foils (100 μm in thickness) with a purity of 99.5%. Ion implantation was performed at 100 keV with monocharged aluminium ions; the beam current was 4 $\mu A\,cm^{-2}$. The maximum dose was $1 \times 10^{17} Al^+\,cm^{-2}$, corresponding to several $\mu g\,cm^{-2}$. The temperature rise never exceeded 300° C during the treatment.

2.1.2. Recoil ion implantation

Aluminium was also implanted into iron by ionic bombardment of a thin predeposited layer. 100 nm of aluminium were deposited onto iron by thermal evaporation. Argon ions were used for the bombardment. An incident dose of $5 \times 10^{16} Ar^+\,cm^{-2}$ (200 keV, 4 $\mu A\,cm^{-2}$) was necessary to achieve the same implantation dose as by direct ion implantation, i.e. $1 \times 10^{17} Al^+\,cm^{-2}$. In order to show that argon implantation does not modify the behaviour of the surface alloy produced, we performed also two successive direct implantations:

$5 \times 10^{16} Ar^+\,cm^{-2}$

$1 \times 10^{17} Al^+\,cm^{-2}$

Three kinds of iron samples were therefore produced:

(a) directly implanted with aluminium ($10^{17} Al^+\,cm^{-2}$);

(b) directly implanted with argon then with aluminium ($5 \times 10^{16} Ar^+\,cm^{-2} + 10^{17} Al^+\,cm^{-2}$); and

(c) recoil implanted with aluminium ($5 \times 10^{16} Ar^+\,cm^{-2} + 10^{17} Al^+\,cm^{-2}$).

2.2. Laser treatment

The continuous wave (CW) Nd–YAG laser used in this study has been described previously [5, 6]. It operates at a wavelength of 1.06 μm, with a maximum power of 30 W. The laser beam collimated to an area of 400 μm in diameter is fixed and the sample moves in front of it with a speed of 1 cm sec^{-1}. The duration of the illumination of a definite point of the metal surface is therefore 40 msec. To prevent any deformation of the sample during the treatment, thick foils were used (1.5 mm).

Small grains of aluminium (< 30 μm in diameter) were added to pure ethanol at a concentration of 50 g $litre^{-1}$. After ultrasonic mixing, the suspension was deposited onto the iron samples ($\sim 0.2\,cm^3\,cm^{-2}$) and the ethanol allowed to evaporate. The aluminium grains were observed to have a uniform repartition on the metal surface with coverage ratio of 90 to 100%.

To prevent thermal oxidation during the treatment, argon was used as a shield gas.

0022–2461/86 $03.00 + .12

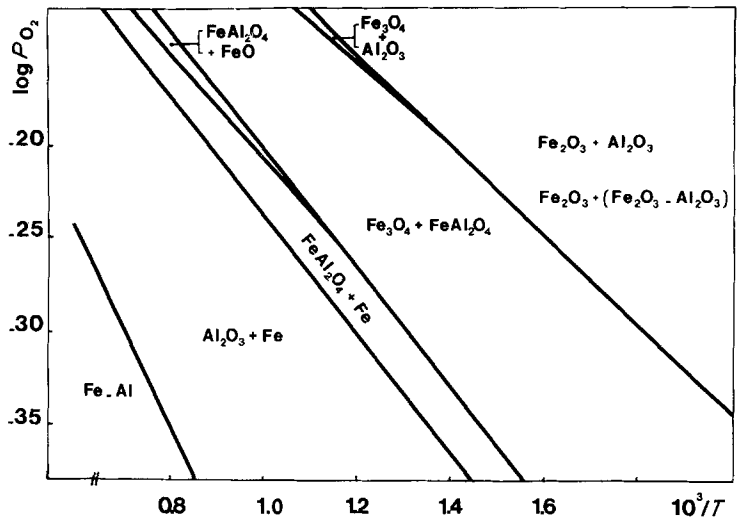

Figure 1 Equilibrium oxygen pressures against temperature of the different oxidized compounds.

3. The iron–aluminium and iron–aluminium–oxygen systems

The iron–aluminium phase diagram [7] shows the high solubility of aluminium in iron (~ 50 at %).

The aluminium concentration needed to form the compounds $FeAl_2$, Fe_2Al_5 or $FeAl_3$ may be achieved by laser alloying but not by ion implantation. For lower concentrations, the thermal effect of laser alloying may induce the formation of the ordered solid solutions Fe_3Al and FeAl. No ordering must occur during the implantation process.

The compounds that could appear during the oxidation of Fe–Al surface alloys are: iron oxides: FeO, Fe_3O_4, Fe_2O_3; alumina: Al_2O_3; and ternary oxides of aluminium and iron.

The only iron–aluminium oxide unambiguously stable under our experimental conditions is the spinel phase $FeAl_2O_4$. The two modifications of the compound $Fe_2O_3 \cdot Al_2O_3$ which were first reported to exist above 1300° C only, are possibly stable at much lower temperatures [8].

If the oxidation process is diffusion-controlled (i.e. all interfacial reactions are at equilibrium) the distribution of all these compounds in all oxidation scale depends on their free enthalpy of formation (or transformation). A diagram log $P(O_2)$ (equilibrium) against $1/T$ is therefore a good way to summarize the results. Such a diagram (Fig. 1) was drawn using the thermochemical data from Barin and Knacke [9]. No data were published concerning $Fe_2O_3 \cdot Al_2O_3$ and we assumed that the two modifications of this compound can be found in the field where both Fe_2O_3 and Al_2O_3 are stable.

Fe_2O_3 + Al_2O_3 or / and (Fe_2O_3-Al_2O_3)	Fe_3O_4 + $FeAl_2O_4$	Fe + $FeAl_2O_4$	Fe + Al_2O_3	Fe-Al

Figure 2 Theoretical succession of the stable phases formed during oxidation of an Fe–Al alloy, $T < 570°$ C (the rate-limiting step is supposed to be only diffusion).

The diagram shows that alumina is the stable phase in contact with the metallic matrix containing aluminium. The spinel phase can form either in the metal or in the lowest oxides but cannot be found mixed with haematite. The compound $Fe_2O_3 \cdot Al_2O_3$ must form directly in contact with the gas phase. These results are summarized by the schematic diagram in Fig. 2, drawn for temperatures lower than 570° C.

4. Study of the iron samples after treatment

The microscopic and profiling techniques have been described in the first paper [5].

4.1. After direct aluminium implantation

The aluminium profile obtained by secondary ion mass spectrometry (SIMS) is given in Fig. 3. The projected range measured on this graph is in good agreement with the theoretical calculations.

The superficial concentration of aluminium lies between 4 and 5 at % for a dose of 10^{17} at cm^{-2} showing evidence of some iron preferential sputtering during the implantation process.

4.2. After recoil implantation

The aluminium profile obtained by glow discharge optical spectrometry (GDOS) is given by Fig. 4. The superficial concentration of aluminium is much higher that that achieved by direct implantation. Recoil implantation allows to go beyond the solubility limit of aluminium in iron (~ 50 at %); however no crystallized iron aluminides could be detected by glancing X-ray diffraction (GXRD).

4.3. After laser treatment

The observations of cross-sections of samples aluminized by laser alloying with a power density of 2.5×10^8 W m^{-2} and a scan rate of 1 cm sec^{-1}, show three different zones (Fig. 5):

a near surface region, containing all aluminium, with a thickness of 20 μm;

a coarse-grained intermediate region, melted during the treatment but where no Fe–Al mixing occurred; and

the iron substrate not affected by the treatment.

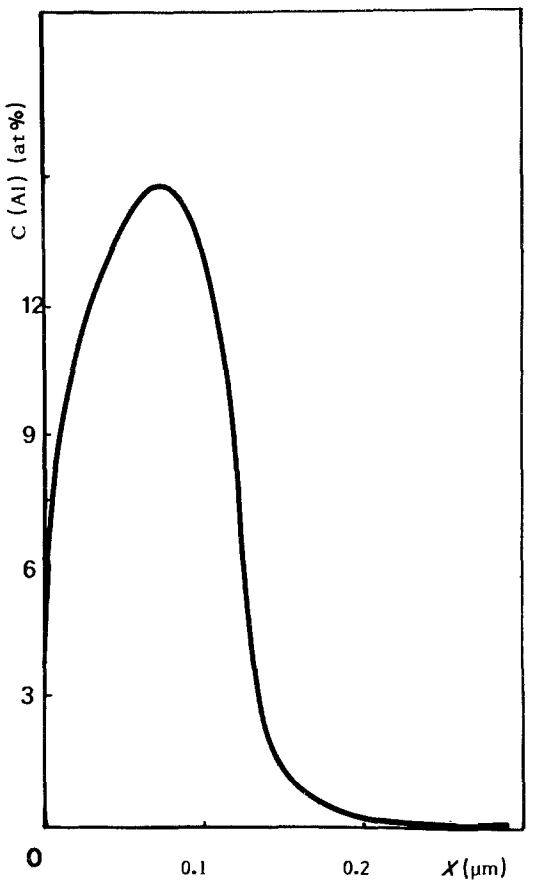

Figure 3 Aluminium profile after implantation (SIMS examination).

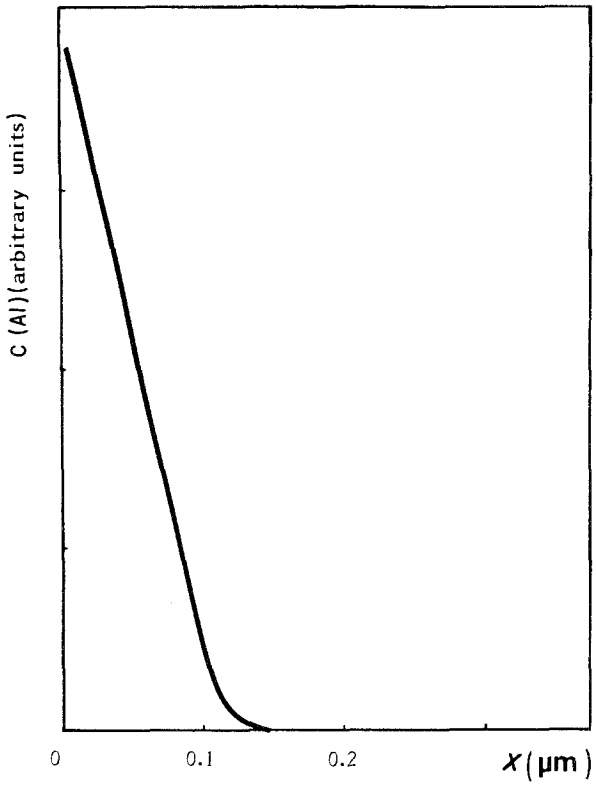

Figure 4 Aluminium profile after recoil implantation (GDOS examination).

The results obtained are therefore quite comparable to those obtained in the Fe–B system [5] for the distribution of the elements. However, the aluminized surface alloy is more homogeneous than the boronized one. This fact is probably due to the high thermal conductivity of aluminium, allowing its complete melting during the treatment. On the contrary, the high absorptivity but low thermal conductivity of boron leads only to its partial melting during laser irradiation.

X-ray diffraction analysis showed the presence of the "compound" FeAl (ordered solid solution). Energy dispersive spectrometry (EDS) performed on the scanning electron microscope showed that, in the aluminized region, the aluminium concentration is about 50 at %.

The results of the two treatments can therefore be resumed as follows:

(i) direct ion implantation (100 keV, $4\,\mu A\,cm^{-2}$, 300° C, $1 \times 10^{17} Al^{+}\,cm^{-2}$) leads certainly to the formation of a solid solution, where the aluminium concentration is maximum (16 at %) at a depth of about 100 nm, and falls to zero at about 200 nm.

(ii) recoil ion implantation ($5 \times 10^{16} Ar^{+}\,cm^{-2}$, 200 keV, $1 \times 10^{17} Al\,cm^{-2}$) leads to a high surface concentration of aluminium which decreases rapidly to zero at a depth of about 100 nm.

(iii) laser alloying (power density: $2.5 \times 10^{8}\,W\,m^{-2}$, interaction time: 0.04 sec) leads to the formation of an aluminized layer to a depth of 20 μm. The aluminium

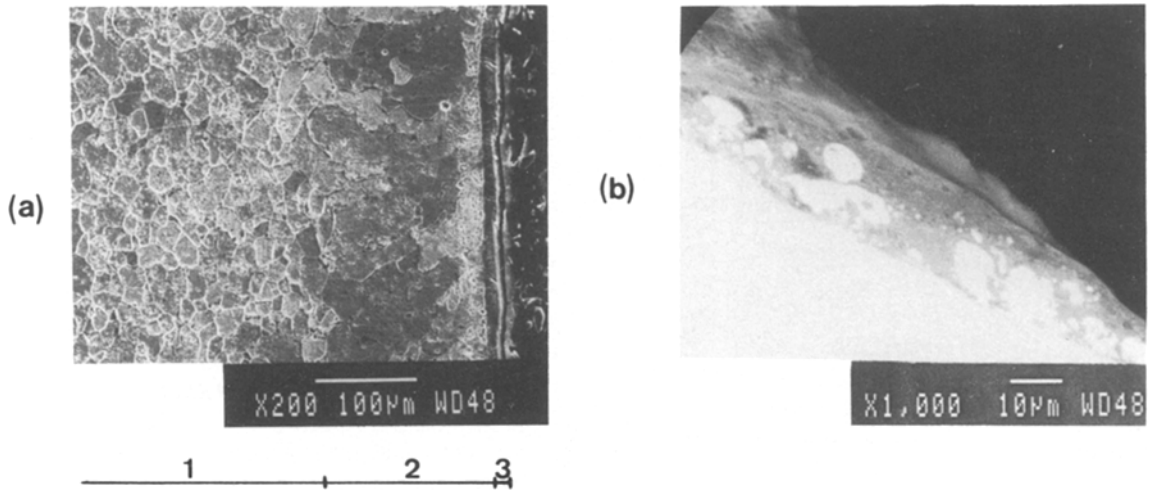

Figure 5 Microscopic examinations of cross-sections of aluminized iron. (a) general view, (b) aluminized zone. 1–Non melted zone, 2–melted zone and 3–aluminized zone.

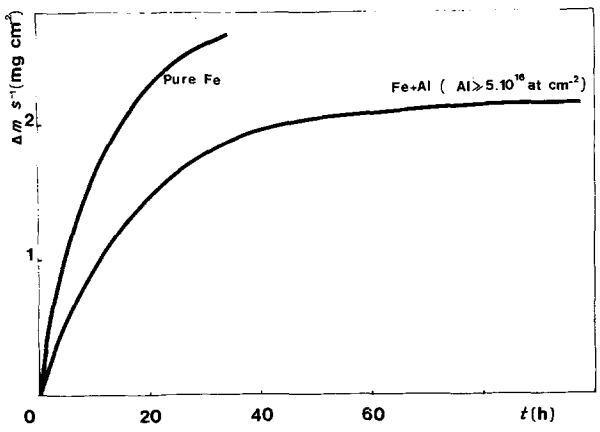

Figure 6 Long time oxidation test of iron implanted at doses higher than 5×10^{16} at cm^{-2}. P_{O_2} = 100 torr; T = 540° C.

concentration in this region is about 50 at %, much higher than in the implanted samples.

The quantities introduced by laser alloying are higher than that involved by ion implantation by three orders of magnitude.

5. Thermal oxidation kinetics

Aluminium implantation was shown to improve considerably the oxidation behaviour of pure iron, as soon as the dose reaches 5×10^{16} at cm^{-2} [10]. At higher doses, the efficiency of the treatment does not depend on the dose up to 1.5×10^{17} at cm^{-2}, the highest dose studied. Fig. 6 shows that after 20 h exposure, the reaction rate decreases very quickly and becomes quite negligible even after 120 h exposure.

The samples treated by recoil implantation or by direct implantation of argon and aluminium exhibited the same behaviour. We may think that defects created by the energetic bombardment have no influence during the high temperature oxidation of iron. The shape of the aluminium profile is also of little importance.

The protection was observed in the 400 to 700° C temperature range [10].

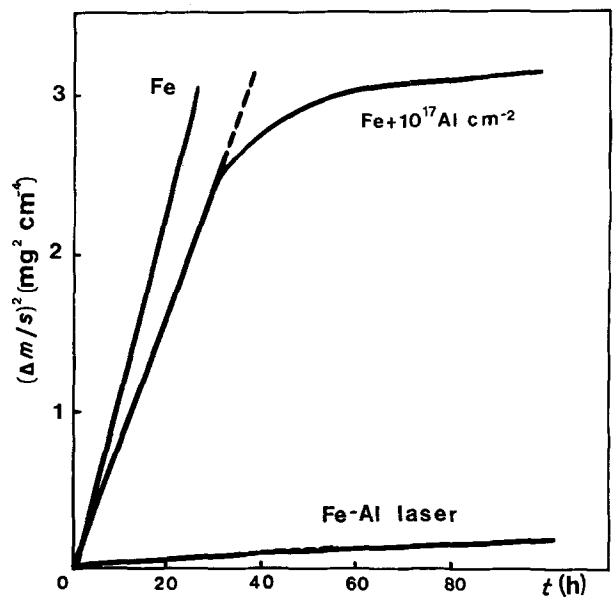

Figure 7 Comparison between ion implantation and laser alloying, parabolic plots. P_{O_2} = 100 torr; T = 500° C.

Aluminium laser alloying was also observed to improve the corrosion resistance of iron in the 400 to 900° C temperature range. As shown in Fig. 7 the protection is much greater than that afforded by ion implantation.

5.1. Beginning of the oxidation

We have already pointed out, for boron alloying [5], that for technical reasons, the iron foils used for implantation experiments had to be thin, whereas those used for laser treatments had to be thicker. Both kinds of iron oxidized parabolically, but some discrepancies were observed on the parabolic constants. However, the measured activation energies were always the same.

Both kinds of aluminized samples oxidized parabolically during a few hours (20 h at 500° C, 8 h at 700° C). An Arrhenius diagram can represent the comparative results of the two treatments (Fig. 8). It must be pointed out that laser alloying is much more effective than implantation during the first few hours of the oxidation. The measured activation energy for the oxidation of laser aluminized samples is almost the same as that for the oxidation of the laser boronized samples [5]. It can be also seen that the parabolic rate constants for pure iron and for aluminium implanted iron oxidation exhibit two different activation energies, whereas the constant concerning the oxidation of the laser aluminized samples exhibits only one activation energy. Table I summarizes the results.

5.2. Extended times of oxidation

After the initial parabolic period, the rate of reaction of the aluminized samples, obtained by ion implantation or laser alloying, diminished more than required by a parabolic law (see Figs 6 and 7). The protection afforded by laser aluminizing is one of the same magnitude as that observed with conventional Fe–5 wt % Al alloys [11, 12] in the 400 to 700° C temperature range. For temperatures above 700° C the protection is less effective.

6. Nature and distribution of the formed oxidized products

6.1. Oxidation of the ion-aluminized samples

Glancing X-ray diffraction experiments (~ 10°) showed that the nature of the phases formed during oxidation depended upon the duration of the reaction. For short oxidation times (t < 1 h), magnetite, haematite and $Fe_2O_3 \cdot Al_2O_3$ described by Atlas and Sumida [8] were observed. With increasing oxidation time, the spinel phase $FeAl_2O_4$ could be identified on the rear face of the oxidation layer after removing it. These results were confirmed by the aluminium profile obtained by secondary ion mass spectrometry (SIMS) which showed a little surface peak corresponding to $Fe_2O_3 \cdot Al_2O_3$ and a more important peak located at the matrix– scale interface corresponding to $FeAl_2O_4$ (Fig. 9). The ion micrographs showed that this last phase was concentrated in form of aggregates, typically 1 to 2 μm in diameter, either in the metal or in the Fe_3O_4 phase. For extended times of reaction (t > 20 h), the spinel phase was the only aluminium containing

TABLE I Oxidation of pure or aluminized iron: activation energies on the parabolic rate constants ($kJ\,mol^{-1}$)

Temperature (°C)	pure Fe (0.1 mm)	pure Fe (1.5 mm)	Fe + $10^{17}\,Al^{+}\,cm^{-2}$ implanted	(Fe–Al) laser alloyed
400	85	75	96	160
600	225	230	200	
800				

compound observed, always located at the metal–oxide interface.

6.2. Oxidation of laser alloyed iron

In this case the nature of the formed products was not dependent on the duration of the reaction.

Whatever the temperature and the duration of the oxidation may be, alumina (Al_2O_3) and $FeAl_2O_4$ were found in the oxidized layer.

The location, in the corrosion scale, of these aluminium-containing phases were found to be: (i) for Al_2O_3: in contact with the metal substrate; and (ii) for $FeAl_2O_4$: mixed with Fe_3O_4 and Fe_2O_3 in the overall oxide scale.

The nature and the location of the formed products are compared for both treatments in Table II.

It must be noted that FeO was never observed after oxidation of laser alloyed iron, even at temperatures where it is stable, contrary to what observed on pure or implanted iron.

It is also easy to see from Table II that the aluminium-containing oxidized phases are located in the overall oxidation layer for laser alloyed iron and only near the metal–scale interface for implanted iron. The difference could account for the observed difference in protection efficiency.

7. Discussion

Laser surface aluminizing has been shown to have a greater efficiency than aluminium implantation against the thermal oxidation of iron. The aluminium containing oxidized phase is responsible for the inhibition of the outward iron diffusion; this protective phase is (a) $FeAl_2O_4$ for aluminium-implanted iron, (b) Al_2O_3 for laser alloying.

In the case of the aluminium implanted specimens, due to the very low amount of aluminium involved, $FeAl_2O_4$ is entirely trapped in the voids formed in the substrate by the interfacial reaction (jump of the iron atoms from the metal to the corrosion scale). FeO is therefore normally observed above its decomposition temperature.

For the laser aluminized samples, Al_2O_3 and $FeAl_2O_4$ are observed in the whole corrosion scale, as the result

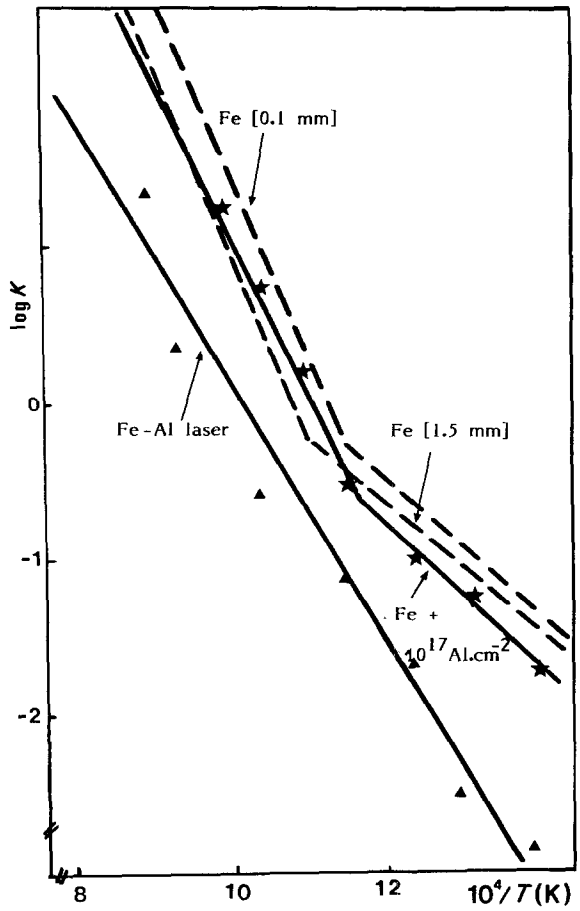

Figure 8 Arrhenius plot for the parabolic rate constant K (oxidation time < 5 h). (▲) Fe–Al laser; (★) Fe + 10^{17} A cm^{-2}; K values were fitted by least squares method.

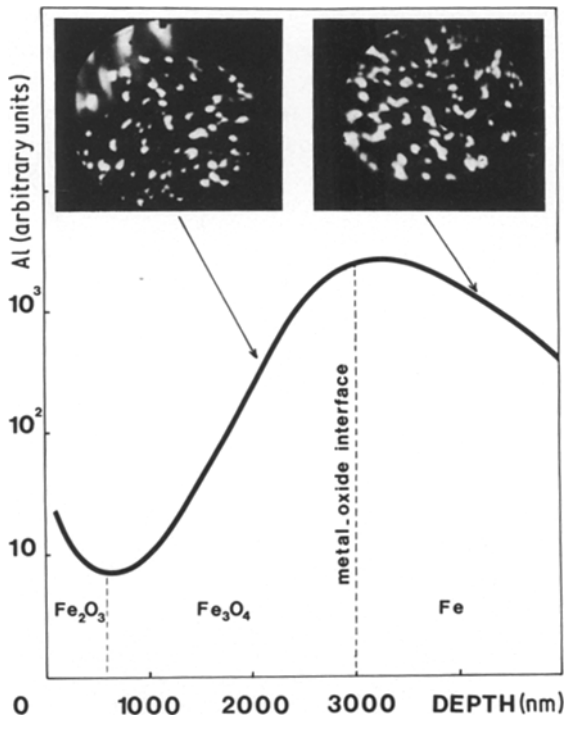

Figure 9 Aluminium profile after 3 h oxidation at 540° C of iron implanted with 1 × $10^{17}\,Al^{+}\,cm^{-2}$ (SIMS profile).

TABLE II Nature and location of the formed products at the end of the oxidation experiments (50 h)

Implantation	Laser alloying	Location
$FeAl_2O_4$	Al_2O_3	Metal–scale interface
FeO ($T \geqslant 600°C$)	Fe_3O_4, Fe_2O_3	
Fe_3O_4	$FeAl_2O_4$	Scale
Fe_2O_3		

of the high aluminium amount introduced by the treatment. $FeAl_2O_4$ is formed from Al_2O_3 (see Figs 1 and 2) by

$$FeO + Al_2O_3 \rightarrow FeAl_2O_4$$

This mechanism certainly accounts for the absence of FeO in the scale.

8. Conclusions

Laser surface alloying and ion implantation of boron and aluminium are efficient to protect iron against high temperature oxidation. Both techniques allow the base metal to be surface-modified and lead to the synthesis of surface-localized alloys. The modified zones and the ways of incorporation are quite different according to the technique used.

Our results concerning boron implantation have shown that small boron contents can drastically inhibit the iron oxidation. When greater quantities are needed, ion beam mixing could be a way to increase implant concentration and therefore the protection. The potential of this technique has been shown in some cases [13, 14].

In the case of laser aluminization of iron, larger amounts of aluminium were shown to be necessary to achieve excellent protection. Further work is needed in this case to improve the compactness and the homogeneity of the surface alloy to achieve the best protection. The mixing mechanism has yet to be understood. It is known that the laser mixing driving force is the surface tension gradient resulting from the thermal gradient. A convection flow develops in the melt pool, and the high velocity involved (one or two orders of magnitude greater than the laser scanning speed [15]) can account for the uniform distribution observed. Several problems arise concerning the mass transfer resistance, during melting, between the two liquid phases. Our work is in progress to correlate the mixing process, driven by heat and mass transports, with the physical and thermochemical properties of the substrate and coating in the liquid state and the process parameters.

References

1. V. ASWORTH, W. A. GRANT and R. P. M. PROCTER, (eds) in "Ion Implantation into Metals" (Pergamon Press, Oxford, 1982).
2. E. Mc CAFFERTY, C. R. CLAYTON and J. OUDAR, (eds) in "Fundamentals Aspects of Corrosion Protection by Surface Modifications" (The Electrochemical Society, Pennington, New Jersey, 1984).
3. K. MUKHERJEE and J. MAZUMDER, (eds) in "Lasers in Metallurgy" (The Metallurgical Society of AIME, Warrendale, Pennyslvania, 1981).
4. M. F. KIMMIT (ed.), in "Lasers in Manufacturing", (North Holland and IFS, Amsterdam, 1983).
5. M. PONS, A. GALERIE and M. CAILLET, *J. Mater. Sci.* **21** (1986) 2697.
6. M. PONS, thèse d'Etat, Institut National Polytechnique of Grenoble, France, (1985).
7. M. HANSEN, in "Constitution of Binary Alloys", (McGraw-Hill, New York, 1958) p. 90; 1st Supplement, R. P. Elliot (1965) p. 35; 2nd Supplement F. A. Shunk (1969) p. 24.
8. L. M. ATLAS and W. K. SUMIDA, *J. Amer. Ceram. Soc.* **41** (1958) 150.
9. I. BARIN and O. KNACKE, "Thermochemical Properties of Inorganic Compounds", (Springer Verlag, Berlin, 1973).
10. M. PONS, M. CAILLET and A. GALERIE, *Nucl. Inst. Meth.* **209/210** (1983) 1011.
11. P. TOMAZEWICK and G. R. WALWORK, *Rev. High Temp. Mater.* **4** (1983) 165.
12. W. BOGGS, *J. Electrochem. Soc.* **118** (1971) 906.
13. A. GALERIE and G. DEARNALEY, *Nucl. Inst. Meth.* **209/210** (1983) 823.
14. *Idem, Mater. Sci. Eng.* **69** (1985) 381.
15. C. CHAN, J. MAZUMDER and M. M. CHEN, *Metall. Trans.* **15A** (1984) 2175.

Received 20 December 1985
and accepted 11 February 1986